Appl Phys B (2010) 99: 163–172
DOI 10.1007/s00340-009-3787-2

Applied Physics B
Lasers and Optics

Effects of angular pump mismatch for the semi-linear oscillator

R. Rebhi · P. Mathey · H.R. Jauslin · B. Sturman

Received: 3 September 2009 / Revised version: 1 October 2009 / Published online: 1 November 2009

Abstract We investigate, analytically and numerically, the influence of an angular mismatch of counter-propagating pump beams on the threshold of oscillation for the photorefractive semi-linear oscillator driven by non-local non-linear response. Our analysis includes the frequency degenerate and non-degenerate regimes within a wide range of the variable input parameters—the coupling strength, the pump ratio, and the feedback mirror reflectivity. The limiting case of mirrorless oscillation is considered as well. The main outcome of our studies is the possibility of strong reduction of the oscillation threshold owing to the angular mismatch. Furthermore, increasing the mismatch induces pronounced bifurcations of the oscillation parameters, including transitions between degenerate and non-degenerate oscillation modes. The main findings are verified by direct simulations of the dynamic equations.

PACS 42.65.Hw · 05.45.-a · 42.65.Pc · 42.65.Sf

1 Introduction

The semi-linear oscillator is the simplest representative of a wide variety of photorefractive (PR) optical oscillators [1–5]. It consists of an ordinary feedback mirror M and a PR crystal which is pumped by two counter-propagating light beams of the same frequency; see Fig. 1. The optical oscillation occurs above a certain threshold owing to the phase conjugation [6, 7] via recording of dynamic index gratings and Bragg diffraction from these gratings [3, 4]. This oscillation is frequency degenerate on the optical scale—the frequency of the oscillating beams is practically the same as the pump frequency.

Despite its simplicity, the semi-linear oscillator shows a rich dynamics, including optical bifurcations, mode competition, and transition to chaos [8–12]. It serves often as a sample for the studies of dynamic non-linear processes. Among the still unclear features of this device is an unexpectedly low threshold for the so-called non-degenerate oscillation, which is characterized by the presence of small, $\lesssim 10^2$ Hz, frequency detunings between the pump and oscillating waves [13, 14].

Most of experimental and theoretical studies of the semi-linear and other photorefractive oscillators are performed for the so-called non-local PR response, which is driven by diffusion of photo-excited charge carriers and characterized by a real coupling constant [3, 4]. Numerical simulations for this case have shown recently that the threshold lowering can be caused by a strong impact of small angular mismatches between the pump waves [15]. The roots of this effect can be found in the previous numerical studies of the influence of the pump mismatch on the phase conjugation and also in studies of the parametric four-wave scattering [16–19].

In this paper, we analyze analytically and numerically the effect of the pump mismatch. The corresponding results are of a great generality. They supplement and generalize the previous numerical data for the non-local PR response.

R. Rebhi · P. Mathey (✉) · H.R. Jauslin
Institut Carnot de Bourgogne, UMR 5209 CNRS-Université de Bourgogne, 9 Avenue Alain Savary, BP 47870, 21078 Dijon Cedex, France
e-mail: pmathey@u-bourgogne.fr

B. Sturman
Institute of Automation and Electrometry of Russian Academy of Sciences, Koptyug Avenue 1, 630090 Novosibirsk, Russia

2 Basic relations

2.1 Wave and grating vectors

The following considerations correspond to the two-dimensional geometric scheme of Fig. 1. Here x is the transversal coordinate ranging from $-\infty$ to ∞ along the input face, and z is the longitudinal (interaction) coordinate ranging from 0 to the crystal thickness l. An important feature of this scheme is the spatial uniformity in x. The spatial dependences are reduced thus to dependences on the propagation coordinate z. In accordance with the scheme, we suppose that pump waves 1 and 2 are incident onto the opposite faces of a sample, $z = 0$ and $z = l$, respectively. Their wave vectors inside the crystal, $\mathbf{k}_1$ and $\mathbf{k}_2$, are almost, but not exactly, opposite to each other. Wave 4 is also incident onto the face $z = l$, its wave vector $\mathbf{k}_4$ inside the crystal is expected to have an arbitrary orientation in the x, z plane. As a result, a phase conjugated wave appears whose wave vector $\mathbf{k}_3$ is almost, but not exactly, opposite to $\mathbf{k}_4$. Our first goal is to determine the wave vector $\mathbf{k}_3$. In the photorefractive case in question, we can restrict ourselves to waves of the same optical frequency and polarization. This means without loss of generality that $k_{1,2,3,4} \equiv |\mathbf{k}_{1,2,3,4}| = 2\pi n/\lambda$, where λ is the vacuum wavelength and n is the background refractive index. The influence of frequency detunings $\lesssim 10^2$ Hz between the waves, i.e., of slow movement of the light-interference fringes, is crucial for the PR response but negligible for $k_{1,2,3,4}$.

The photorefractive four-wave coupling occurs generally via transmission (T) and reflection (R) index gratings [3–5]. The wave vector $\mathbf{k}_3$ can be determined in the general case without specification of the grating type. It is necessary to realize merely that the phase-matching condition $\mathbf{k}_1 + \mathbf{k}_2 = \mathbf{k}_3 + \mathbf{k}_4$, which gives $\mathbf{k}_3 = -\mathbf{k}_4$ for exactly counter-propagating pump waves, irrespectively of the type of the PR gratings, must be replaced by the condition $k_{1x} + k_{2x} = k_{3x} + k_{4x}$ in the presence of angular mismatch. The latter condition can be treated as a conservation law; it is dictated by the uniformity along the coordinate x. Combined with the equality $k_{1,2,3,4} = 2\pi n/\lambda$, it allows one to express easily the propagation angle for wave 3 via the propagation angles for the incident waves 1, 2, and 4. The combination

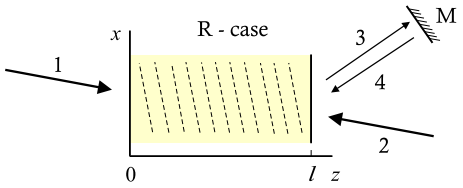

Fig. 1 Geometric scheme of the semi-linear oscillator. The *parallel dashed lines* illustrate the grating fringes of the reflection grating, M is the ordinary feedback mirror, and l is the crystal thickness

$\Delta = k_{1z} + k_{2z} - k_{3z} - k_{4z}$ is non-zero in the general case. This important parameter characterizes the Bragg mismatch for both T- and R-cases. It is easily expressed by the angular mismatch for one of the pump beams $\delta\theta_p$,

$$\Delta \simeq \frac{2\pi}{\lambda n}(\sin\theta_p + \sin\theta_o)\delta\theta_p, \tag{1}$$

where θ_p and θ_o are the non-perturbed values of the pump and oscillation angles measured from the normal. All angles are given in air. Furthermore, the angular correction for the angle θ_3 (in air) is $\delta\theta_3 \simeq \delta\theta_p$.

Generally, the pump mismatch can lead also to the appearance of small y-components of the wave vectors (out-of-plane distortions). In this case, we must use additionally the strict phase-matching condition $k_{4y} = k_{1y} + k_{2y} - k_{3y}$ to get a more complicated, compared to (1), particular expression for the main mismatch parameter Δ. All subsequent relations remain unchanged.

Consider now the necessary relations for the grating vectors. Reflection gratings can be recorded by the wave pairs 1, 4 and 3, 2, see Fig. 1. The corresponding grating vectors, $\mathbf{K}_{14} = \mathbf{k}_1 - \mathbf{k}_4$ and $\mathbf{K}_{32} = \mathbf{k}_3 - \mathbf{k}_2$, are equal to each other only at zero pump mismatch, when $\Delta = 0$. Otherwise, they are not exactly the same. This means that diffraction of wave 3 from the $\mathbf{K}_{14}$ grating, as well as diffraction of wave 4 from the $\mathbf{K}_{32}$ grating, is slightly off-Bragg. At the same time, we have generally $\mathbf{K}_{14,x} = \mathbf{K}_{32,x}$ owing to the above conservation law. The same properties are inherent in the transmission gratings formed by the wave pairs 1, 3 and 4, 2.

2.2 Slowly-varying amplitudes

The light electric field E_l can be represented as

$$E_l = \sum_{s=1}^{4} A_s e^{i\mathbf{k}_s\cdot\mathbf{r} - i\omega t} + c.c., \tag{2}$$

where $A_{1,2,3,4} = A_{1,2,3,4}(z,t)$ are slowly-varying complex amplitudes of the light waves, ω is the light frequency, and $c.c.$ indicates complex conjugation. However, this definition is not unique. In particular, the variables $\tilde{A}_{3,4} = A_{3,4}\exp(-i\Delta z/2)$ can equally be regarded as slowly varying amplitudes of waves 3, 4 because the factor $\exp(-i\Delta z/2)$ is a slowly varying function of z.

Consider now the implications of this circumstance for the description of the grating recording which is determined by the intensity modulation. The light intensity modulation produced by the wave pair 1, 4 is given by

$$A_1 A_4^* e^{iK_{14,x}x + iK_{14,z}z} + c.c.$$
$$= A_1 \tilde{A}_4^* e^{iK_{14,x}x} e^{i(K_{14,z} - \Delta/2)z} + c.c. \tag{3}$$

Similarly, the intensity modulation coming from the wave pair 3, 2 is

$$A_3 A_2^* e^{iK_{32,x}x + iK_{32,z}z} + c.c. = \tilde{A}_3 A_2^* e^{iK_{32,x}x} e^{i(K_{14,z} - \Delta/2)z} + c.c. \quad (4)$$

As we know, $K_{14,x} = K_{32,x}$. Furthermore, one can check straightforwardly that $K_{14,z} - \Delta/2 = K_{32,z} + \Delta/2$. The spatial dependence of the intensity modulation is thus the same in the right-hand sides of (3) and (4). It is natural to denote $K_x = K_{14,x} = K_{32,x}$, $K_z = K_{14,z} - \Delta/2 = K_{32,z} + \Delta/2$, and refer to the vector $\mathbf{K} = (K_x, K_z)$ as the common grating vector for the wave pairs 1, 4 and 3, 2. Correspondingly, the space-charge field E_{sc} produced by the wave pairs 1, 4 and 3, 2 can be represented as

$$E_{sc} = E_K e^{i\mathbf{K}\cdot\mathbf{r}} + c.c., \quad (5)$$

where E_K is the grating amplitude.

2.3 Dynamic equations

It is clear from the above considerations that the necessary modifications of the known dynamic equations for the light amplitudes are reduced to the replacement $A_{3,4} \to \tilde{A}_{3,4}$ and to the addition of the term $i(\Delta/2)\tilde{A}_{3,4}$ to the left-hand side of the equations for $\tilde{A}_{3,4}$ to account for the exponential z-dependence of these amplitudes in the absence of gratings. For the R-geometry and the non-local PR response, we obtain, using the known equations for $\Delta = 0$ [1, 3, 12],

$$\begin{aligned}
&\frac{\partial A_1}{\partial z} = u^* \tilde{A}_4,\\
&\frac{\partial A_2}{\partial z} = u \tilde{A}_3,\\
&\left(\frac{\partial}{\partial z} + \frac{i\Delta}{2}\right)\tilde{A}_3 = u^* A_2,\\
&\left(\frac{\partial}{\partial z} + \frac{i\Delta}{2}\right)\tilde{A}_4 = u A_1,\\
&t_r \frac{\partial u}{\partial t} + u = \frac{\gamma}{I_0}\left(A_1^* \tilde{A}_4 + A_2 \tilde{A}_3^*\right).
\end{aligned} \quad (6)$$

Here u is the effective grating amplitude, γ is a real coupling constant, $I_0 = I_1 + I_2 + I_3 + I_4$ is the total light intensity, $I_s = |A_s^2|$ is the intensity of the s-th wave, and $t_r \propto 1/I_0$ is the time of the photorefractive response [3, 4].

It is not difficult to rewrite this set of equations in terms of the amplitudes $A_{3,4}$; this leads to the appearance of the exponent $\exp(-i\Delta z/2)$ in the right-hand sides [20]. Our equivalent form of the dynamic equations is preferable for the subsequent analysis.

The above modification procedure of the dynamic equations is fully applicable to the T-case. Moreover, the results obtained below for the R-case can be easily rewritten for the T-case.

Note finally that the definition of the mismatch as $|k_{1z} + k_{2z} - k_{3z} - k_{4z}|$, used in [15], includes the symbol of absolute value, which restricts artificially the range of variations of Δ.

3 General characteristics

3.1 Undepleted pump approximation

In this important case, which implies smallness of the oscillation amplitudes, the pump amplitudes can be treated as constants, $A_1 = A_1^0$ and $A_2 = A_2^l$, and we have from (6) a closed system of linear differential equations for $\tilde{A}_3^*$, $\tilde{A}_4$, and u:

$$\begin{aligned}
&\left(\frac{\partial}{\partial z} - \frac{i\Delta}{2}\right)\tilde{A}_3^* = u A_2^*,\\
&\left(\frac{\partial}{\partial z} + \frac{i\Delta}{2}\right)\tilde{A}_4 = u A_1,\\
&t_r \frac{\partial u}{\partial t} + u = \frac{\gamma}{I_0}\left(A_1^* \tilde{A}_4 + A_2 \tilde{A}_3^*\right),
\end{aligned} \quad (7)$$

where t_r is a constant determined by the input pump intensity $I_0 = I_1 + I_2$. These equations admit a solution $\tilde{A}_3^*, \tilde{A}_4, u \propto \exp(-i\Omega t)$ with an arbitrary frequency detuning Ω. The grating amplitude is algebraically expressed then by the light amplitudes,

$$u = \frac{\gamma}{I_0(1 - i\Omega t_r)}\left(A_1^* \tilde{A}_4 + A_2 \tilde{A}_3^*\right). \quad (8)$$

The resulting set of ordinary linear differential equations for $\tilde{A}_3^*$ and $\tilde{A}_4$ can be written in matrix form:

$$\frac{d}{dz}\begin{pmatrix}\tilde{A}_3^*\\ \tilde{A}_4\end{pmatrix} = \begin{pmatrix}S_{33} & S_{34}\\ S_{43} & S_{44}\end{pmatrix}\begin{pmatrix}\tilde{A}_3^*\\ \tilde{A}_4\end{pmatrix}. \quad (9)$$

The matrix elements are given by

$$\begin{aligned}
S_{33} &= \frac{\gamma |A_2|^2}{I_0(1 - i\Omega t_r)} + \frac{i\Delta}{2}, \qquad S_{34} = \frac{\gamma A_1^* A_2^*}{I_0(1 - i\Omega t_r)},\\
S_{44} &= \frac{\gamma |A_1|^2}{I_0(1 - i\Omega t_r)} - \frac{i\Delta}{2}, \qquad S_{43} = \frac{\gamma A_1 A_2}{I_0(1 - i\Omega t_r)}.
\end{aligned} \quad (10)$$

The diagonal elements S_{33} and S_{44}, which account for the two-beam coupling effects [4], depend on the mismatch Δ, but do not depend on the pump-wave phases. The non-diagonal elements S_{34} and S_{43} account for the parametric effects [17]. They depend on the phases, but do not depend on Δ.

3.2 Phase conjugate reflectivity

Equation (9) admits solutions $\tilde{A}_3^*, \tilde{A}_4 \propto \exp(\Gamma z)$, where the characteristic exponent Γ satisfies the standard characteristic equation and takes two values,

$$\Gamma_\pm = h \pm \sqrt{h^2 - d} \tag{11}$$

with $h = (S_{33} + S_{44})/2$ and $d = S_{33}S_{44} - S_{34}S_{43}$ being the half-trace and the determinant of the $\hat{S}$-matrix, respectively. As seen from (10), h does not depend on the mismatch Δ, and $\Gamma_\pm$ does not depend on the phases of the pump waves. The general solution of (9) is

$$\begin{pmatrix} \tilde{A}_3^* \\ \tilde{A}_4 \end{pmatrix} = c_+ \begin{pmatrix} \Gamma_+ - S_{44} \\ S_{43} \end{pmatrix} e^{\Gamma_+ z} + c_- \begin{pmatrix} \Gamma_- - S_{44} \\ S_{43} \end{pmatrix} e^{\Gamma_- z}, \tag{12}$$

where $c_\pm$ are two arbitrary constants.

Using the boundary condition for the semi-linear oscillator $\tilde{A}_3^*(0) = 0$, see Fig. 1, we easily calculate an important characteristic [1, 4]—the amplitude reflection coefficient $\rho = \tilde{A}_3^*(l)/\tilde{A}_4(l)$ characterizing the phase conjugation:

$$\rho = \frac{S_{43}^{-1}(e^{\Gamma_+ l} - e^{\Gamma_- l})}{(\Gamma_+ - S_{44})^{-1} e^{\Gamma_+ l} - (\Gamma_- - S_{44})^{-1} e^{\Gamma_- l}}. \tag{13}$$

At first sight, this expression has no expected symmetry in the matrix indices. It is necessary to keep in mind, however, that $(\Gamma - S_{44})/S_{43} = S_{34}/(\Gamma - S_{33})$ according to the characteristic equation for Γ. Thus, ρ can be reexpressed by $(\Gamma_\pm - S_{33})/S_{34}$, which displays the necessary symmetry.

As follows from the definition of ρ, the frequency detuning for the phase conjugate wave 3 is opposite to that of the incident wave 4. This is indeed a general feature of the phase conjugation [6, 7].

3.3 Threshold equations

To obtain the threshold equation for the semi-linear oscillator, we have to take into account the ordinary feedback mirror M (see Fig. 1). This means fulfilment of the boundary condition $\tilde{A}_4(l) = \sqrt{R}\tilde{A}_3(l)$, where R is the mirror reflectivity. Introduction of an arbitrary phase factor in the right-hand side of this condition gives no new results [14].

The physics of the oscillation can be clarified if we recall the mentioned feature of the phase conjugation—inversion of the frequency detuning. The component of the incident wave 4 detuned by $-\Omega$ $[\tilde{A}_4^-(l) \propto \exp(-i\Omega t)]$ gives the conjugate reflected signal $[\tilde{A}_3^+(l) \propto \exp(+i\Omega t)]$. After a reflection from the ordinary mirror M, it transforms into the incident component $\tilde{A}_4^+(l) \propto \exp(+i\Omega t)$. After the next phase conjugation, we obtain the signal $\tilde{A}_3^-(l) \propto \exp(-i\Omega t)$ which must be transformed to the initial signal after the second ordinary reflection. In short, the sequence of the elementary processes is $\tilde{A}_4^- \to \tilde{A}_3^+ \to \tilde{A}_4^+ \to \tilde{A}_3^- \to \tilde{A}_4^-$.

In accordance with this consideration, we represent the amplitudes $\tilde{A}_{3,4}^l$ in the form

$$\tilde{A}_{3,4}^l = c_{3,4}^+ e^{+i\Omega t} + c_{3,4}^- e^{-i\Omega t}. \tag{14}$$

Then we have the obvious relations

$$\frac{c_3^{+*}}{c_4^-} = \rho(\Omega, \Delta), \qquad \frac{c_3^{-*}}{c_4^+} = \rho(-\Omega, \Delta), \qquad \frac{c_4^\pm}{c_3^\pm} = \sqrt{R}, \tag{15}$$

where $\rho = \rho(\Omega, \Delta)$ is given by (13). By combining these relations, we obtain the threshold equation in the general form:

$$\rho(\Omega, \Delta)\rho^*(-\Omega, \Delta)R = 1. \tag{16}$$

The only difference of this equation from the previous general threshold equation [14] is the dependence of ρ on the mismatch Δ. This difference is, however, very important.

To make the general equation (16) practically useful for analysis of the pump mismatch, we reshape the expression (13) for ρ.

– First, we introduce the normalized/dimensionless variable parameters

$$g = \gamma l, \qquad \nu = \Omega t_r, \qquad \delta = \Delta/2\gamma, \qquad r = I_2/I_1. \tag{17}$$

The parameter g is the coupling strength, ν is the normalized frequency detuning, δ is the normalized mismatch, and r is the pump ratio. Instead of δ one can use the normalized mismatch $\tilde{\delta} = \Delta l = 2g\delta$. The choice between δ and $\tilde{\delta}$ is a matter of convenience. The subsequent analytical expressions are shorter in terms of δ, while the use of $\tilde{\delta}$ is preferable for the graphics. For any particular combination of the experimental parameters λ, θ_p, θ_o, n and l, the normalized mismatch Δl (or $\Delta/2\gamma$) can be readily expressed by the angular mismatch $\delta\theta_p$ using (1), see, e.g., Sect. 5.

– Second, we express, using (10), the phase conjugate reflectivity in terms of g, r, $\Phi_p = \arg(A_1 A_2)$, and three functions (f, Q_+, and Q_-) of ν, δ, and r,

$$\rho = \frac{\exp(-i\Phi_p)}{\sqrt{r}} \frac{\sinh(gf)}{Q_+ \exp(gf) - Q_- \exp(-gf)}. \tag{18}$$

The functions $f(\nu, \delta, r)$ and $Q_\pm(\nu, \delta, r)$ are given by

$$f = \left[\frac{1}{4(1 - i\nu)^2} + \frac{i\delta(r-1)}{(1-i\nu)(r+1)} - \delta^2 \right]^{1/2},$$
$$Q_\pm = \left[r - 1 + 2(r+1)(1 - i\nu)(i\delta \pm f) \right]^{-1}. \tag{19}$$

The pump phase Φ_p does not enter the threshold equation (16) and can be omitted without loss of generality.

With the dependence $\rho(g, \delta, \nu, r)$ specified, we have a firm basis for the threshold analysis. We have the complex *transcendental* threshold equation (16), which is equivalent to two real equations. It gives generally a sequence of branches for the pair of functions $g(\delta, r, R)$ and $\nu(\delta, r, R)$. As follows from the symmetry properties, the branches of $g(\delta)$ and $\nu(\delta)$ are symmetric with respect to the mirror reflection about the vertical axis $\delta = 0$. Furthermore, the branches of $\nu(\delta)$ are symmetric with respect to the mirror reflection about the horizontal axis $\nu = 0$. We will see below particular examples of the symmetry properties of the branches.

In the special case $\delta = 0$ (zero mismatch) we have $f = 1/2(1 - i\nu)$, $Q_+ = 1/2r$, $Q_- = -1/2$, and, correspondingly,

$$\rho = \sqrt{r} e^{-i\Phi_p} \frac{1 - \exp[-\gamma l/(1 - i\Omega t_r)]}{1 + r \exp[-\gamma l/(1 - i\Omega t_r)]}. \tag{20}$$

This is a known result, see [14].

The general symmetry property of ρ, $\rho(\nu, \delta) = \rho^*(-\nu, -\delta)$, which follows from (18) and (19), is useful. It allows one to rewrite the threshold equation (16) as $\rho(g, \nu, r, \delta)\rho(g, \nu, r, -\delta)R = 1$ or, alternatively, as $\rho(g, \nu, r, \delta)\rho(g, -\nu, r, \delta)R = 1$. It is thus even in both δ and ν. Let a combination g, ν, δ, r, R satisfy the threshold equation. Then, as follows from the symmetry properties, the combinations $g, -\nu, \delta, r, R$, $g, \nu, -\delta, r, R$, and $g, -\nu, -\delta, r, R$ also satisfy it. In particular, we always have two opposite values of the detuning, $\nu = \pm|\nu(\delta, r, R)|$, for each value of $g(\delta, r, R)$.

In contrast to the particular case $\delta = 0$, where $\rho(\nu)\rho^*(-\nu) = \rho^2(\nu)$, the threshold equation cannot generally be split into two separate equations. This makes the analysis of the case $\delta \neq 0$ more complicated.

In accordance with (18), the phase conjugate reflectivity $\rho(g, \nu, \delta, r)$ goes to infinity at the zeros of the denominator. These points satisfy the complex equation

$$g = \frac{1}{2f} \ln\left(\frac{Q_-}{Q_+}\right). \tag{21}$$

It corresponds to the threshold of the mirrorless optical oscillation [21, 22]. This oscillation can be viewed as a limiting case of the "semi-linear" oscillation for $R \to 0$. However, there is a subtle difference. In accordance with the symmetry property of $\rho(\nu, \delta)$, we have only two equivalent combinations of the threshold parameters for the mirrorless oscillation, g, ν, δ, r and $g, -\nu, -\delta, r$, instead of four combinations for the semi-linear oscillator. The difference comes from the mentioned two-fold transformation $\Omega \to -\Omega \to \Omega$ in the semi-linear oscillator, which occurs owing to the ordinary mirror and symmetrizes (in ν) the threshold properties.

4 Threshold analysis

Numerical analysis of the general complex transcendental equation (16) with $\rho(g, \nu, \delta, r, R)$ given by (18) and(19) is not an easy task. An efficient method is to plot contour lines of $|\rho(\delta)\rho(-\delta)R - 1|$ on the (g, ν) plane. The zeros of this absolute value, which correspond to the solutions for g and ν with the other parameters fixed, can be easily determined in this way. By varying δ (or, alternatively, $\tilde{\delta} = \Delta l$), one can plot the threshold values of g and ν as functions of Δl for different combinations of R and r. Similarly, one can analyze (21) for the mirrorless-oscillation threshold.

Before coming to an analysis of the impact of the angular mismatch Δ on the threshold characteristics, it is useful to summarize what is known for $\Delta = 0$ [14].

4.1 Zero-mismatch threshold characteristics

For $\Delta = 0$, we have a sequence of branches for $g(r, R)$ and $\nu(r, R) = \pm|\nu|(r, R)$. Solid lines 0, 1, and -1 in Fig. 2 (their numbering is a matter of convenience) show the lowest branches of $g(r)$ for $R = 0.1$. Branch 0 corresponds to $\nu = 0$, i.e., to a degenerate oscillation. With decreasing R, this branch shifts up and to the right, and the minimum value of $g(r)$ goes to infinity for $R \to 0$. Branches ± 1 correspond to non-degenerate oscillations, i.e., to $|\nu| \neq 0$. The minimum values of $g(r)$ for these branches are the same and independent of R: $g_{\min} = 2\pi$. With decreasing R, branches 1 and -1 approach each other. Their limit for $R \to 0$, shown by the dotted line, corresponds to the mirrorless oscillation. The non-degenerate oscillation can thus be viewed as the mirrorless oscillation perturbed by the feedback mirror.

Figure 3 shows the R-dependences of the optimum (minimizing g) pump ratio for branches 0, 1, and -1. For branches 1 and -1, we have $r_{\min} = \exp(\pi)$ at $R = 0$, which corresponds to the mirrorless oscillation. For $R \neq 0$, the ± 1 branches are separated, and the separation grows initially extremely fast with R. For sufficiently small values of R, the

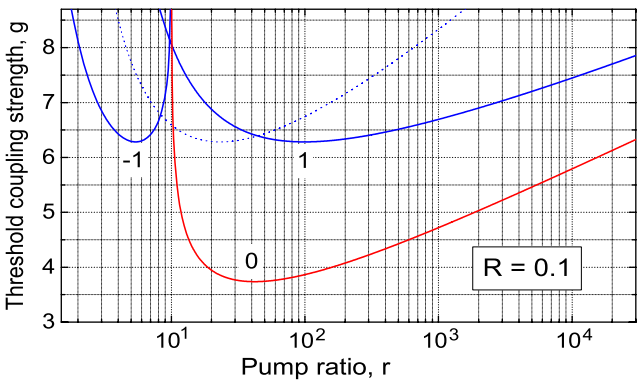

Fig. 2 Degenerate (0) and non-degenerate (± 1) branches of $g(r)$ for $R = 0.1$. The *dotted line* corresponds to $R = 0$

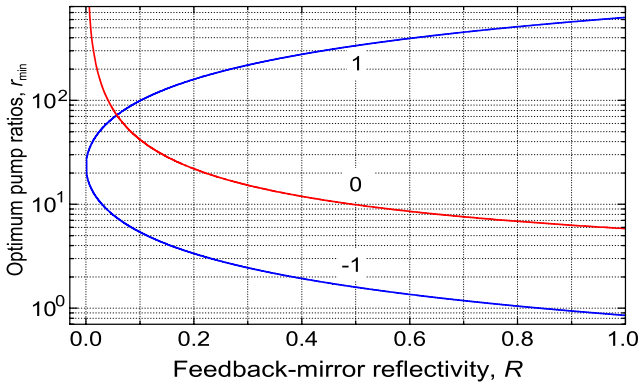

Fig. 3 The optimum pump ratio for the branches 0, 1, and −1 versus the reflectivity R

non-degenerate branches are also well separated from the degenerate branch 0.

In addition to the 0 and ±1 branches, shown in Fig. 2, there are branches with much higher values of the coupling strength g. Usually, they are of minor interest.

4.2 Mirrorless-oscillation thresholds for $\Delta \neq 0$

Since the mirrorless oscillation is closely related to the non-degenerate regime of the semi-linear oscillator, it is natural to consider first the impact of the pump mismatch on the mirrorless-oscillation threshold. This case is the simplest because it is free from particularities of the external feedback loop. Furthermore, it is expected to be important for the analysis of numerous oscillation schemes based on phase conjugation [1–5].

Figure 4a shows the lowest branches of $g(\Delta l)$ for the pump ratio $r = 5$, and Fig. 4b gives the corresponding values of $\nu(\Delta l)$. The most striking feature is a strong decrease of the threshold coupling strength with increasing pump mismatch: the value of g decreases from $\simeq 7.74$ to $\simeq 3.73$! The last number is almost two times smaller than the minimum threshold value of the coupling strength for zero angular detuning, $g_{\min} = 2\pi$.

The structure of the branches in Fig. 4 is remarkable. We have a sequence of branches $g_j(\Delta l)$ and $\nu_j(\Delta l)$ with $j = \pm 1, \pm 2, \pm 3, \ldots$; the minimum value of $g_j(\Delta l)$ increases with increasing $|j|$. The branches with $j < 0$ and $j > 0$ are linked by the symmetry relations: $g_j(-\Delta l) = g_{-j}(\Delta l)$ and $\nu_j(-\Delta l) = -\nu_{-j}(\Delta l)$. They fully comply with the symmetry properties of $\rho(\nu, \delta)$. Remarkably, the mirrorless oscillation with a zero frequency detuning ($\nu = 0$) is possible for $\Delta \neq 0$; the coupling strength g is close to its local minima in this case. Only quantitative changes occur with the above branches when changing the pump ratio r.

A natural question arises: what is the absolute minimum of the threshold value of the coupling strength g as a function of Δl and r? Our numerical analysis has shown, see

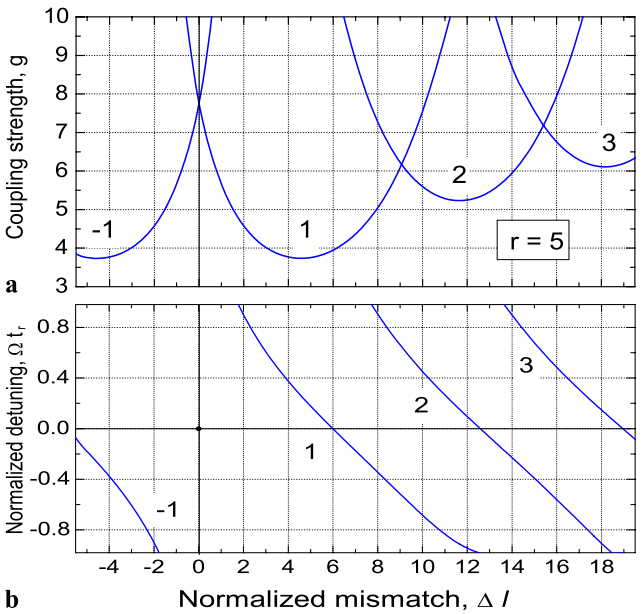

Fig. 4 Threshold values of the coupling strength (**a**) and the normalized frequency detuning (**b**) versus the normalized mismatch for the mirrorless oscillation at $r = 5$. Only the lowest branches $j = -1, 1, 2, 3$ are shown

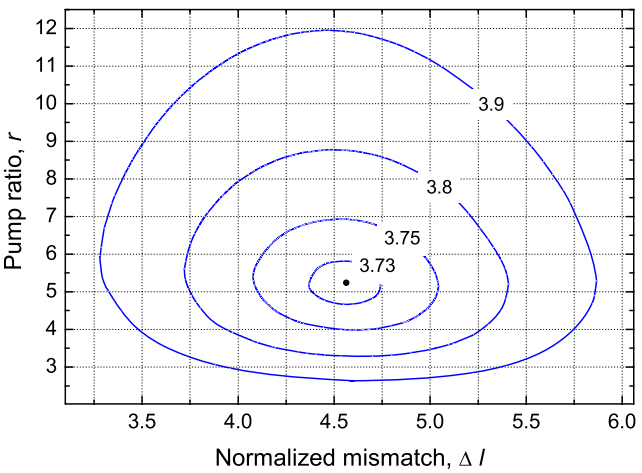

Fig. 5 Contour plots $g(\Delta l, r) = 3.73$, 3.75, 3.8, and 3.9 illustrating the absolute minimum of the coupling strength for the mirrorless oscillation. The *cental dot* corresponds to $g \simeq 3.726$

Fig. 5, that *the absolute minimum* is $g_{\min}^{\text{abs}} \simeq 3.726$. It corresponds to $r \simeq 5.244$ and $\Delta l \simeq 4.563$. The normalized frequency detuning for these control parameters is $\nu \simeq 0.257$. The same value of g and the opposite value of ν occur indeed for $\Delta l \simeq -4.563$. An almost *twofold decrease* of the threshold coupling strength is thus achievable by introducing proper angular mismatches. Note that the value $r = \exp(\pi) \simeq 23$, minimizing g at $\Delta = 0$, is far from 5.244. On the other hand, the value $r = 5$ in Fig. 4 is close to the pump ratio realizing the absolute minimum of g.

4.3 Semi-linear oscillator thresholds for $\Delta \neq 0$

Because of an additional variable parameter R, this case is more complicated to exhaust. In what follows, we restrict ourselves to representative examples.

The first example is for $R = 0.5$ and $r = 336$. For $\Delta = 0$, the degenerate branch 0 coexists with the non-degenerate branch 1 (compare to Fig. 2) and we have initially $g_0 \simeq 3.373$, $\nu_0 = 0$, $g_1 \simeq g_1^{\min} = 2\pi$, and $\nu_1 \simeq \pm 1$. The mismatch does not affect the quality of the oscillation to be degenerate, $\nu_0(\Delta l) = 0$, so that the effect of Δl is reduced to quantitative changes. As follows from Fig. 6, the mismatch makes the threshold of the degenerate oscillation higher. The situation with the non-degenerate oscillation is the opposite. The value of the coupling strength g_1 first decreases with $|\Delta l|$ and then increases; the minimum of $g_1(\Delta l)$ is pronounced—$g_{\min}/g(0) \simeq 0.9$. The absolute value of the frequency detuning for branch 1 decreases monotonically with increasing Δl.

Note that the above dependences are even in Δl, which differs from the symmetry properties of the branches $g(\Delta l)$ and $\nu(\Delta l)$ for the mirrorless oscillation; see Fig. 4. This in full agreement with the general symmetry properties of the threshold equations indicated in Sect. 3C.

Consider now a qualitatively different example of the threshold behavior. It is for $R = 0.4$ and $r = 2$, which corresponds to $g_{-1} \simeq 2\pi$ and $\nu_{-1} \simeq \pm 1$ at $\Delta = 0$, see also Fig. 2. The main feature of this choice is that the degenerate oscillation is absent for zero mismatch.

As one can see from Fig. 7, the situation is entirely different here. For sufficiently small mismatches, we still have a single solution for the threshold coupling strength; the value of g_{-1} decreases with Δl together with the corresponding value of $|\nu_{-1}|$. At $\Delta l = (\Delta l)_c \simeq 4.2$ a bifurcation takes place: for $\Delta l > (\Delta l)_c$ we have two solutions for g and a single zero solution for ν, which corresponds to a new frequency degenerate oscillation labelled by 0. The frequency non-degenerate mode transforms thus in a critical manner into a frequency degenerate one. For $\Delta l > (\Delta l)_c$, the value of $g_0(\Delta l)$ decreases for the lowest sub-branch, reaches a minimum ($g_{\min} \simeq 3.59$), and then starts to grow. This growth is not monotonic, it is accompanied by oscillations. The values of g and ν for $\Delta l < 0$ can be obtained, as before, by the mirror reflection of the curves in Fig. 7 about the vertical axis $\Delta l = 0$.

The last example illustrates the transition to the mirrorless oscillation when decreasing the reflectivity R. This transition is also accompanied by non-trivial qualitative changes. Figure 8 shows the lowest branches of $g(\Delta l)$ for $r = 5$ and $R = 0.01$. It is instructive to compare it with Fig. 4a plotted for $r = 5$ and $R = 0$. First, the expected split of the branches of g appears at $\Delta l = 0$. Second, bifurcations of the branches, which correspond to transitions between the frequency non-degenerate and degenerate oscillations, occur around $\Delta l \approx 6$, 13, and 19. The degenerate oscillation appears thus via bifurcations when R increases starting from zero. Numerous branches $\nu(\Delta l) = \pm|\nu(\Delta l)|$ are not shown in Fig. 8.

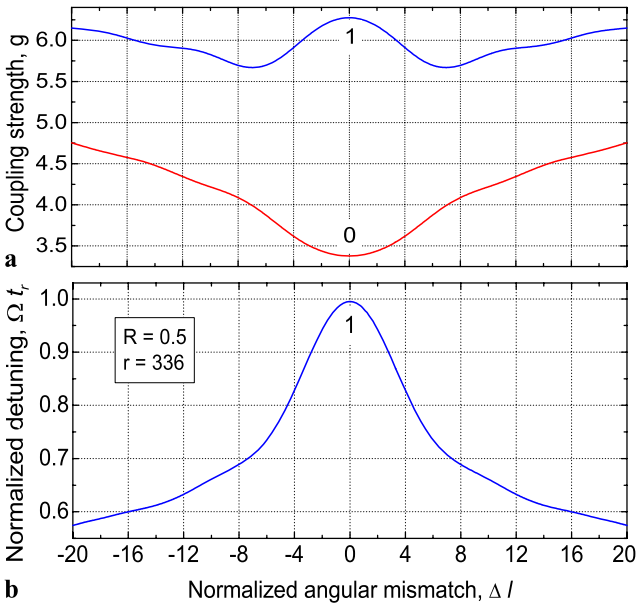

Fig. 6 Threshold values of the coupling strength (**a**) and of the frequency detuning (**b**) versus the normalized mismatch Δl for $R = 0.5$ and $r = 336$; curves 0 and 1 correspond to the degenerate and non-degenerate branches, respectively

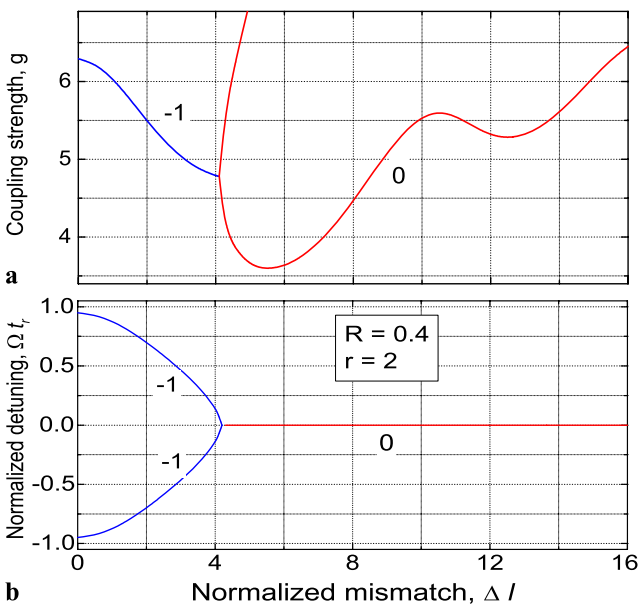

Fig. 7 The threshold values of the coupling strength g (**a**) and of the normalized detuning ν (**b**) versus the normalized mismatch Δl for $R = 0.4$ and $r = 2$. Numbers -1 and 0 indicate the old non-degenerate and new degenerate branches

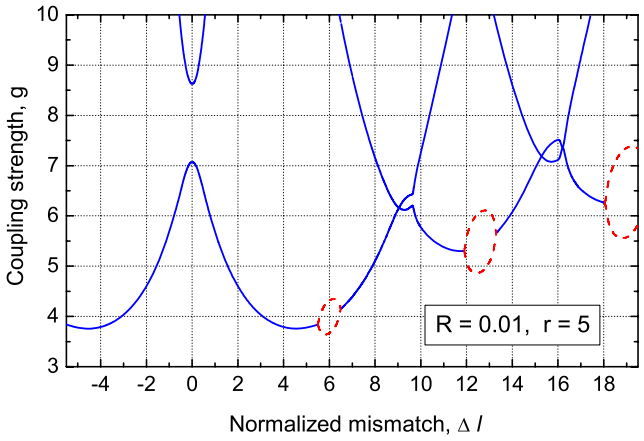

Fig. 8 Threshold coupling strength versus the normalized mismatch for $R = 0.01$ and $r = 5$. The *solid* and *dashed lines* correspond to non-degenerate ($|\nu| \neq 0$) and degenerate ($\nu = 0$) branches, respectively

4.4 Comparison with direct simulations

To verify the correctness of the above analysis and to gain a different view of the threshold behavior, we have simulated directly the initial set (6) of non-linear dynamic equations. This set was solved with the zero boundary values of the oscillation amplitudes, $A_3(0,t) = 0$, $A_4(l,t) = 0$, and a very small random initial value of the grating amplitude $u(z,0)$, see [12] for more details. This seed value initiates the oscillation but, as we have checked, does not influence the steady state. No particular values of the frequency detuning were thus imposed in our numerical simulations. The time behavior of the amplitudes is fully determined by the structure of the non-linear equations.

In all cases considered, the temporal behavior changes sharply when crossing the expected threshold of g. Below the threshold, we always have a zero steady state for $I_{3,4}(t)$, while above the threshold we have a pronounced steady-state oscillation. Moreover, it is easy to see whether the oscillation is degenerate or not. Two representative examples are given in Fig. 9. In case (a), the input parameters are $R = 0.01$, $r = 5$, $\Delta l = 4.5$, and $g = 3.9$. We are slightly above the threshold here in accordance with Fig. 8, and the expected oscillation is non-degenerate. As one can see from Fig. 9a, the steady-state behavior of $I_3(l)$, which takes place for $t/t_r \gtrsim 300$ just corresponds to this oscillation mode. Moreover, the period of the oscillation, $\simeq 11.07$, corresponds to the relevant threshold value, $\nu \simeq 0.258$, in Fig. 8. Small changes of the input parameters in case (b), $g \to 3.8$ and $\Delta l \to 6$, bring us to the region of the expected degenerate oscillation. The numerical results of Fig. 9b with no steady-state oscillations of $I_3(l)$ are in a full agreement with the threshold analysis.

Note that the contrast of the intensity modulation is not unity in Fig. 9a. This means that the constants c_3^+ and c_3^- in (14) have different absolute values. Furthermore, it is easy to find from (15) that $|c_3^+|^2/|c_3^-|^2 = |\rho(\Delta l, \nu)|/|\rho(\Delta l, -\nu)$. This ratio is not unity for $\Delta l \neq 0$. The mentioned feature of the intensity modulation is thus also the effect of the angular detuning. One can show that the value of the modulation contrast is in a good agreement with the threshold characteristics.

5 Discussion

A strong influence of small angular mismatches between the pump beams on the threshold characteristics of the semilinear oscillator is highly remarkable. This influence is not reduced to small corrections of the oscillation thresholds. Instead, it can lead to strong reduction of these thresholds. In particular, the minimum threshold value of the coupling strength for the mirrorless oscillation, which was expected to be 2π [13, 14], can be lowered almost by a factor of two owing to angular detunings. This modified value is comparable with the minimum threshold value of the coupling strength for the local photorefractive response, $g_{\min} = \pi$ [1, 21].

It is interesting that an increase of the angular mismatch can be accompanied by non-trivial bifurcations, i.e., by qualitative changes of the oscillation behavior. In particular, the non-degenerate oscillation can become degenerate and vice versa. Generally, bifurcations are typical of non-linear dynamic systems [23], but particularities of the bifurcation behavior are strongly individual.

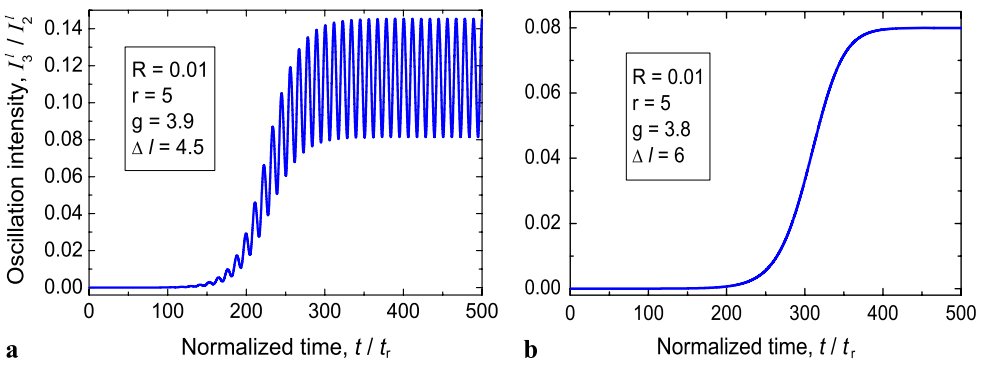

Fig. 9 Time dependence of the intensity ratio I_3^l/I_2^l during the oscillation development for two specified sets of the input parameters. Cases (**a**) and (**b**) correspond to the non-degenerate and degenerate oscillation, respectively

The results of the threshold analysis, obtained within the undepleted pump approximation in the R-case for $g > 0$, admit two useful generalizations. (i) To consider the region of negative coupling strength in the R-case, it is sufficient to replace $g \to -g$ and $r \to 1/r$ in the above relations. (ii) To consider the T-case (dominating transmission gratings) it is sufficient to replace $r \to 1/r$ [12]. These generalizations extend the results known for the case of zero angular and frequency detunings [1].

We have analyzed above the most common case of the non-local (diffusion driven) photorefractive response. One can expect that the influence of the pump mismatch will be essentially different in the case of local response. An increase of the oscillation threshold seems to be most likely in this case.

While the strong effect of the angular detuning is important, it is not completely surprising. Similar mismatch effects are known in the theory of four-wave parametric scattering in photorefractive crystals [17]. The underlying reason is closely related to the compensation of the non-linearly introduced corrections of the wave vectors by the angular mismatches.

It is useful to estimate the angular deviation $\delta\theta_p$ which corresponds to $\Delta l \approx 3$ and is sufficient for the investigated effects. By taking the refractive index $n = 2.3$, the wavelength $\lambda = 514$ nm, the crystal thickness $l = 3$ mm, and the angle $\theta_o = 30°$, we obtain $\delta\theta \approx 2 \times 10^{-2}$ deg.

Focused pump beams, which are often used in the oscillation experiments, have much larger angular divergences. Correspondingly, they comprise plenty of plane-wave pairs with essentially different mismatches. It is difficult to expect a quantitative agreement between the four-wave theory, including only two plane pump waves, and experimental results in this case. Non-focused laser beams have an angular spread because of their finite width. This width has to be large enough, $\gtrsim$1 cm, to ensure a small effect of the angular mismatches. This condition can be achieved but it is not the case of a typical experiment.

Analysis of the oscillation characteristics outside the plane-wave approximation would involve complicated and highly-specialized three-dimensional numerical calculations. This analysis is beyond the scope of this paper.

6 Summary

A general threshold equation for the semi-linear oscillator, including a frequency detuning between the pump and oscillating waves and an angular mismatch between the pump beams, is derived. This complex transcendental equation contains five variable parameters—the coupling strength, the frequency detuning, the angular mismatch, the pump intensity ratio, and the reflectivity of the ordinary feedback mirror. The limiting case of zero reflectivity corresponds to the mirrorless-oscillation threshold.

An analysis of the effect of the pump mismatch on the oscillation thresholds is performed for the mirrorless oscillation and the semi-linear oscillator combining analytical and numerical tools. A strong, almost two-fold, lowering of the threshold coupling strength by introducing the angular mismatch is found.

We predict for certain cases that increasing pump mismatch results in bifurcations of the output characteristics, i.e., in qualitative changes of the oscillation behavior. This includes mutual transformations between degenerate and non-degenerate oscillation modes.

As follows from our results, serious restrictions have to be imposed on the pump beam quality in order to use the plane-wave model for comparison with experimental data. In particular, the use of focused beams has to be excluded and the width of non-focused beams has to be of the order of 1 cm. In the opposite case, the oscillation behavior must be analyzed outside the wide-spread plane-wave approach.

Acknowledgement B. Sturman acknowledges the support of Université de Bourgogne during his stay in Dijon.

References

1. M. Cronin-Golomb, B. Fisher, J.O. White, A. Yariv, IEEE J. Quantum Electron. **20**, 12 (1984)
2. B. Fischer, S. Sternklar, S. Weiss, IEEE J. Quantum Electron. **25**, 550 (1989)
3. P. Günter, J.-P. Huignard (eds.), *Photorefractive Materials and Their Applications II*. Topics in Appl. Phys., vol. 62 (Springer, Berlin, 1989)
4. L. Solymar, D.J. Webb, A. Grunnet-Jepsen, *The Physics and Applications of Photorefractive Materials* (Clarendon, Oxford, 1996)
5. S. Odoulov, M. Soskin, A. Khyzhnyak, *Optical Coherent Oscillators with Degenerate Four-Wave Mixing* (Harwood Academic, Reading, 1991)
6. B.Y. Zel'dovich, N.F. Pilipetsky, V.V. Shkunov, *Principles of Phase Conjugation*. Springer Series in Optical Sciences, vol. 42 (Springer, Berlin, 1985)
7. A. Yariv, P. Yeh, *Optical Waves in Crystals* (Wiley, New York, 2003)
8. S.R. Liu, G. Indebetouw, J. Opt. Soc. Am. B **9**, 1507 (1992)
9. K. Staliunas, M.F.H. Tarroja, G. Slekyus, C.O. Weiss, L. Dumbly, Phys. Rev. A **51**, 4140 (1995)
10. C. Denz, M. Schwab, M. Sedlatchek, T. Tschudi, T. Honda, J. Opt. Soc. Am. B **15**, 2057 (1998)
11. A. Shumelyuk, A. Hryhorashchuk, S. Odoulov, Phys. Rev. A **72**, 023819 (2005)
12. M. Grapinet, P. Mathey, H. Jauslin, B. Sturman, D. Rytz, S. Odoulov, Eur. Phys. J. D **41**, 363 (2007)
13. P. Mathey, S. Odoulov, D. Rytz, J. Opt. Soc. Am. B **19**, 2967 (2002)
14. P. Mathey, M. Grapinet, H.R. Jauslin, B. Sturman, D. Rytz, S. Odoulov, Eur. Phys. J. D **39**, 445 (2006)
15. R. Rebhi, P. Mathey, M. Grapinet, H. Jauslin, S. Odoulov, Appl. Phys. B **91**, 583 (2008)

16. C. Denz, J. Golz, T. Tschudi, Opt. Commun. **72**, 129 (1989)
17. B.I. Sturman, S.G. Odoulov, M.Yu. Goulkov, Phys. Rep. **275**, 197 (1996)
18. R. Rebhi, P. Mathey, H. Jauslin, B.I. Sturman, Opt. Lett. **33**, 2773 (2008)
19. R. Rebhi, P. Mathey, H. Jauslin, G. Cook, D. Evans, D. Rytz, S. Odoulov, Phys. Rev. A **80**, 013803 (2009)
20. N.V. Kukhtarev, T.I. Semenets, K.H. Ringhofer, G. Tomberger, Appl. Phys. B **41**, 259 (1986)
21. A. Yariv, D.M. Pepper, Opt. Lett. **1**, 16 (1977)
22. J. Feinberg, R. Hellwarth, Opt. Lett. **5**, 519 (1980)
23. H. Haken, *Synergetics* (Springer, Berlin, 1978)